ELSEVIER

Polymer 43 (2002) 7007–7015

polymer

www.elsevier.com/locate/polymer

Simulation of the initial development of an inhomogeneous structure upon cooling an elastomeric polypropylene from a homogeneous melt

Guoqiang Xu, Wayne L. Mattice*

Department of Polymer Science, The University of Akron, Akron, OH 44325-3909, USA

Received 15 July 2002; received in revised form 3 September 2002; accepted 4 September 2002

Abstract

The initial development of inhomogeneity upon stepwise cooling from the melt has been investigated in an elastomeric polypropylene (elPP), with isotactic and atactic blocks in the same chain. The simulation employs coarse-grained chains, with one bead for each repeating unit, on a high coordination lattice. Short-range intramolecular interactions are described by a rotational isomeric state model. Intermolecular interactions are derived from the behavior of pairs of molecules of propane in the gas phase. Analysis of the rates of equilibration of the simulations shows that there is sufficient time for local conformational relaxation at all temperatures studied from 298 to 473 K. However, at the lower temperatures there is insufficient time for the more extensive rearrangement of the chains required for development of the intermolecular interactions that would stabilize crystals of the isotactic blocks. Therefore the simulation is appropriate for the investigation of any heterogeneity that might develop before the onset of significant crystallization of the isotactic blocks. The fraction of C–C bonds in different rotational isomeric states changes very little over the temperature range covered. Intermolecular pair correlation functions have similar shapes when calculated for all beads, or for just those beads that appear in isotactic blocks. Nevertheless, there is greater heterogeneity in the elPP at 298 K than in isotactic polypropylene at the same temperature and thermal history. The heterogeneity of elPP can be detected by an analysis of the orientations of pairs of coarse-grained bonds and also from an analysis of the dynamics of individual beads. This heterogeneity of elPP, which appears before the onset of significant crystallization of the isotactic blocks, has contributions from individual 3_1 helices in the isotactic blocks and from strongly extended chain segments in those portions of the atactic blocks that are rich in *racemo* diads.

Keywords: Dynamics; Elastomeric polypropylene; Monte Carlo simulation

1. Introduction

Recent developments in metallocene catalysts provide routes to the synthesis of a variety of stereoregular and partially regular homopolymers and copolymers [1]. Polypropylene (PP) that has isotactic and atactic blocks within a single chain is a notable example. The material is termed elastomeric polypropylene (elPP) because the isotactic blocks can crystallize if they are sufficiently long, but the atactic blocks remain amorphous even at low temperature (T). The stress–strain behavior is different from that observed with isotactic polypropylene (iPP) [2], and the formation of a temperature-dependent physical network is evident in the small amplitude rheology [3].

The properties of elPP depend on the type of catalyst used in its preparation. Some materials, such as those reported by Collins and coworkers [2,4] and by Chien et al. [5], have solubility characteristics that suggest they are homogeneous in isotacticity. In contrast, Waymouth's group has prepared elPP that is heterogeneous in isotacticity, as shown by the separation of a sample with the probability of an isotactic pentad (p_{mmmm}) of 0.32 into three fractions with p_{mmmm} of 0.18, 0.33, and 0.51 [6]. The three fractions and the reconstituted sample have different properties.

Prior simulation of elPP has focused on the production of ordered regions by alignment of crystallizable sequence runs in fully extended chains, represented as strings in two- or three-dimensional arrays [7,8]. The strings are constructed with sequences of diads that reflect the material under investigation. A postulate of the shortest sequence required for formation of a crystallite, along with maximization of the alignment of crystallizable sequence runs by sliding neighboring strings with respect to one another

* Corresponding author. Fax: +1-216-9725396.
E-mail address: wlm@polymer.uakron.edu (W.L. Mattice).

0032-3861/02/$ - see front matter
PII: S0032-3861(02)00641-9

along their axes, provides an estimate of the crystallinity obtainable with the material. The coarse-grained nature of the chains, and their representation as fully extended strings, precludes expression of the model at atomistic detail in continuous three-dimensional space.

A recent simulation of the homogeneity of two-component melts of PP chains that differ in stereochemical composition [9] reproduces the important qualitative features of the miscibility observed experimentally for these melts [10–13]. That simulation employed a method for bridging between coarse-grained and fully atomistic descriptions of a polymer melt [14], in order to provide access to the necessary size and time scales, while retaining the ability to specify the stereochemical sequence of each chain. Individual replicas of the equilibrated coarse-grained systems used in these Monte Carlo simulations can be reverse-mapped to atomistically detailed descriptions of the system in continuous three-dimensional space [9]. The simulation reproduces earlier experimental observations which show that iPP and atactic polypropylene (aPP) are miscible in the melt [10,13], but syndiotactic polypropylene (sPP) is immiscible with either iPP or aPP [11–13]. The simulation also identifies the molecular mechanism responsible for the immiscibility of sPP with either iPP or aPP in the melt [9,15,16].

Given this accomplishment with PP in the melt, it is of interest to inquire what sort of heterogeneity might be detected by the same type of simulation when all of the independent parent chains are assigned stereochemical sequences that mimic those reported for elPP, and the system is cooled from the melt to a T below the melting temperature of iPP. Does the system become heterogeneous only when there is crystallization of the isotactic blocks, or does the system become heterogeneous before crystallization occurs? The result of that simulation is reported here.

2. Simulation method and system

The simulation places eight independent coarse-grained chains, each with 50 beads, on a high coordination lattice with $10i^2 + 2$ sites in shell i and an angle of 60° between any two axes [17,18]. Since each bead represents a $CH_2CH(CH_3)$ unit, the chains reverse map to $C_{150}H_{302}$ [9]. The step length on the lattice, 2.5 Å, is the distance between second nearest neighbor carbon atoms. Occupancy of 11.85% of the sites produces a density of 0.7503 g/cm^3, comparable with the density of iPP at 473 K [19]. All simulations were performed at this density. We thereby ignore the densification that is produced by cooling. Although strict adherence to physical reality makes it desirable to include this property in the simulation, it would come at the cost of a slower equilibration. Since isothermal crystallization is accompanied by an increase in density, our neglect of the densification produced on cooling will tend to delay the onset of crystallization in the simulation. This delay in crystallization is actually somewhat advantageous in a search for the development of heterogeneity prior to the onset of crystallization. Therefore we have kept the same density throughout.

The chains are simulated with a Metropolis Monte Carlo procedure [20], using a Hamiltonian that has two parts. One part is derived from the mapping of a rotational isomeric state model for PP onto the coarse-grained chains [18]. This part of the Hamiltonian enforces the proper distribution of mean square dimensions for each chain, and for its subchains, and also maintains the stereochemical sequence initially assigned to each chain. The specific rotational isomeric state model used is one described by Suter et al. [21]. The second part of the Hamiltonian incorporates the intermolecular interactions. It uses a discrete version of a continuous Lennard-Jones potential energy function with $\varepsilon/k_B = 237.1$ K and $\sigma = 5.118$ Å, which describes the interaction of pairs of molecules of propane [22]. The discretization is performed with the constraint that the continuous function and its discretized version specify the same value of the second virial coefficient for propane [23]. The discretized energies for the first three shells are listed in Table 1. They are temperature-dependent due to the appearance of T in the Mayer f function, which is used in the conversion of the continuous function to a discrete function [23]. The first two shells are repulsive because, with a step length of 2.5 Å on the high coordination lattice, they fall within the distance specified by σ. Higher shells are attractive, with the strongest attraction appearing in the third shell [9]. The energies for the first three shells are used in the simulation. Equilibration uses single bead moves [24] and pivot moves of 2–6 beads [25]. A Monte Carlo step (MCS) is the length of the simulation that attempts one move, on an average, for each bead and each type of move.

The stereochemical sequences of the parent chains were generated using a method similar to the block model of Bravakis et al. [2]. This method produces an alteration between isotactic and atactic blocks in each chain. The atactic blocks are grown using 0.5 as the probability for a *meso* diad. The fraction of monomers in isotactic blocks of four or more consecutive *meso* diads is 0.55. The longest isotactic block contains 19 monomers. The fractions of various pentads are reported in Table 2, and the sequences themselves are listed in Table 3. The fractions of various pentads are similar to those found in elPP samples and used

Table 1
Discrete interaction energies (kJ/mol) for the first three shells

T (K)	First shell	Second shell	Third shell
298	18.181	1.594	−1.168
350	20.836	2.054	−1.141
400	23.318	2.477	−1.118
420	24.923	2.642	−1.110
473	26.837	3.068	−1.089

Table 2
Fractions of various pentads in the parent chains (m = *meso*, r = *racemo*)

Pentad	Fraction
mmmm	0.358
mmmr + *mmrm* + *mrmm* + *rmmm*	0.248
mmrr + *mrrm* + *rrmm* + *rmmr*	0.277
mrmr + *rmrm*	0.043
mrrr + *rmrr* + *rrmr* + *rrrm*	0.057
rrrr	0.016

in computer simulations [26]. For comparison, simulations were also performed for systems in which every chain was iPP.

3. Results and discussion

3.1. Dynamics of the chains and the completeness of the equilibration

A careful consideration of the extent of the equilibration achieved in the simulation is essential to a proper interpretation of the results. The equilibration of the conformations of elPP was studied using the five mean square displacements defined in Eqs. (1)–(5) [27]

$$g_1(t) = \langle[\mathbf{r}_{\text{inner}}(t) - \mathbf{r}_{\text{inner}}(0)]^2\rangle \quad (1)$$

$$g_2(t) = \langle[\mathbf{r}_{\text{inner}}(t) - \mathbf{r}_{\text{cm}}(t) - \mathbf{r}_{\text{inner}}(0) + \mathbf{r}_{\text{cm}}(0)]^2\rangle \quad (2)$$

$$g_3(t) = \langle[\mathbf{r}_{\text{cm}}(t) - \mathbf{r}_{\text{cm}}(0)]^2\rangle \quad (3)$$

$$g_4(t) = \langle[\mathbf{r}_{\text{end}}(t) - \mathbf{r}_{\text{end}}(0)]^2\rangle \quad (4)$$

$$g_5(t) = \langle[\mathbf{r}_{\text{end}}(t) - \mathbf{r}_{\text{cm}}(t) - \mathbf{r}_{\text{end}}(0) + \mathbf{r}_{\text{cm}}(0)]^2\rangle \quad (5)$$

The positions of an internal bead, end bead, and the center of mass of a chain at time t are denoted by $\mathbf{r}_{\text{inner}}(t)$, $\mathbf{r}_{\text{end}}(t)$, and $\mathbf{r}_{\text{cm}}(t)$, respectively. The five $g_i(t)$ for the simulation of elPP at 473 K are depicted in Fig. 1. At short times, $g_1(t)$ and $g_2(t)$ are indistinguishable, as are $g_4(t)$ and $g_5(t)$. As the simulation continues, $g_1(t)$ and $g_4(t)$ increase without limit, but $g_2(t)$ and $g_5(t)$ approach constant values, with the limit for $g_5(t)$ being somewhat larger than the limit for $g_2(t)$. At

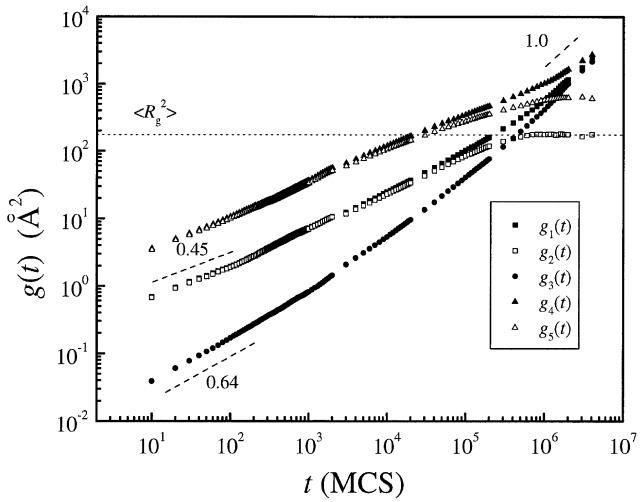

Fig. 1. The $g_i(t)$, defined in Eqs. (1)–(5), for elPP at 473 K. The long horizontal dashed line denotes $\langle R_g^2\rangle$. The three short dashed straight lines have slopes of 0.45, 0.64, and 1.0.

long times, $g_1(t)$, $g_3(t)$ and $g_4(t)$ approach the same value, and this shared value continues to increase throughout the simulation. Their slope at long times approaches 1, as expected for Fickian diffusion. A chain can be considered to have relaxed from its initial conformation when $g_1(t)$, $g_3(t)$ and $g_4(t)$ become identical, and $g_2(t)$ and $g_5(t)$ reach their limiting values. This behavior is not achieved until $g_3(t)$ exceeds the mean square radius of gyration, $\langle R_g^2\rangle$. Nearly the same result (not shown here) is obtained for the $g_i(t)$ in a simulation of iPP with the same degree of polymerization, at the same T.

The mobility of the center of mass decreases strongly at lower T, as shown in Fig. 2. The value of $g_3(t)$ at 4 million MCS is smaller than $\langle R_g^2\rangle$ at $T < 400$ K.

Equilibration of the conformations of the chains was also monitored using the normalized orientation autocorrelation functions (OACF) formulated from the end-to-end vector, $\langle\mathbf{R}(t)\cdot\mathbf{R}(0)\rangle/\langle R^2\rangle$, and the bond vector, $\langle\mathbf{m}(t)\cdot\mathbf{m}(0)\rangle/\langle m^2\rangle$. The bond vector of the coarse-grained model becomes a chord vector in the fully atomistic representation of the chain. The decay of these two OACFs is depicted in Fig. 3. At any T, the OACF defined with $\mathbf{m}$ decays more rapidly than the

Table 3
Stereochemical sequences for the eight parent chains

Chain	Diad sequence
1	*mmmmmrrmrrmmmrmrmrmrmrrmrmmmmmrrmmmrrmmrrrmmmmmmm*
2	*mmmmrrmrrrmmmrrmmmmmmmrrmrrrmmrrmrrmrmmmmmmrrmrrmm*
3	*rrmrrrmmmmmmmmmmrmrmmrrmmrrmmmmmmmmmmrrmmmmmmmmmmmmm*
4	*mmmmmmmmmmmmmmmmmmmmrmmrmrrrmmmmmmmmrrmmmmmmmmmmmmmrm*
5	*mmmmrrmmmmrrmmmmmmmmmmmrrrmmmmmmrrmmmmmrrmmmmmmmmm*
6	*rrrmmmmmmmmmmmmmmmmmmmmrrrmmrmmrmmmmmmmmmmmmmmrrmm*
7	*mmrmrmmmmmmrmrmmrrmmrrrmrmmmmrrmmmmmmmrrmmmmmmm*
8	*rmrrrmmmmmmrrmmmmmmrrrmmrrmmmmrrmmmmrrmrrmmmmmmm*

Sequences of four or more *meso* diads are underlined.

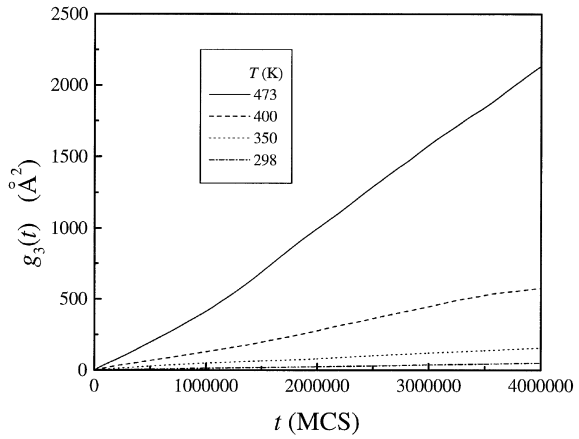

Fig. 2. Mean square displacement of the center of mass of the chains of elPP at four T.

OACF defined with **R**, because the reorientation of a local segment is faster than the reorientation of the chain as a whole. Both types of reorientation are complete within 4 million MCS at 473 K. At the lowest T of 293 K, substantial relaxation of the local chain segment is achieved, with $\langle \mathbf{m}(t)\cdot\mathbf{m}(0)\rangle/\langle m^2\rangle$ falling to a value well below $1/e$. However, there has been only a small relaxation of the orientation of the chain as a whole at 293 K (Fig. 3(b) and $g_3(t)$ has risen to only about 40% of $\langle R_g^2\rangle$ (Fig. 2).

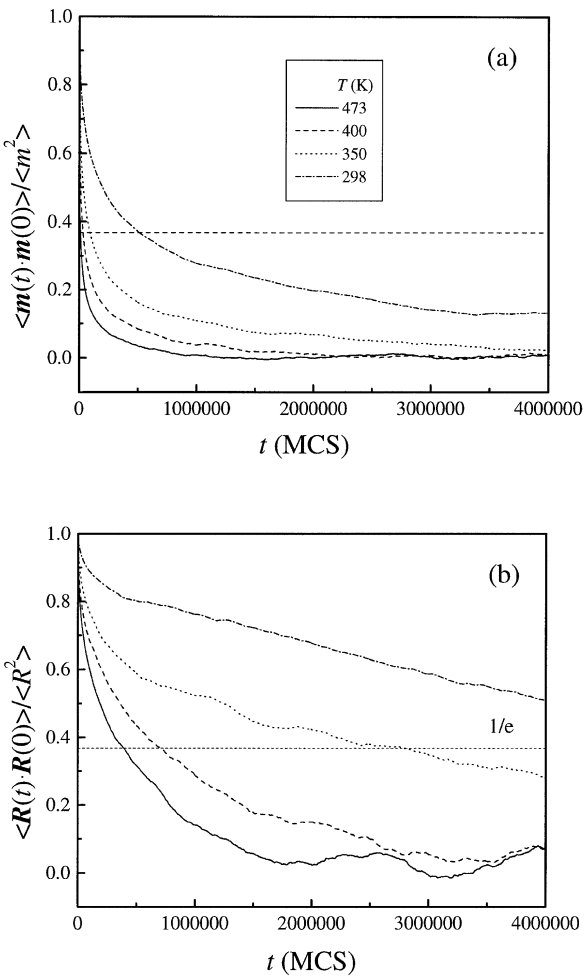

Fig. 3. OACFs for (a) the bond vector, **m**, and (b) the end-to-end vector, **R**, in simulations of elPP at 298, 350, 400, and 473 K. The horizontal dashed lines are $1/e$.

In the simulations reported below, a stepwise cooling is used and 8 million MCS are simulated for the system at each successive T. The systems are well equilibrated [as judged by the behavior of the $g_i(t)$ and the OACFs from **m** and **R**] at $T \geq 400$ K. At lower T, there has been a reasonable equilibration of the local segments (as judged by the OACF defined with **m**), but the equilibration of the system on the distance scale of an entire chain [as judged by the $g_i(t)$ and the OACF defined with **R**] is incomplete. Since equilibration is not achieved on the distance scale of an entire chain at $T < 400$ K, the simulation does not allow sufficient time for the development of mature crystals by the isotactic blocks. The simulation is designed to search for the onset of detectable inhomogeneity before the formation of stable crystals.

3.2. Average local conformation of a chain

The conformations of the underlying C–C bonds can be established unambiguously from the conformation of the coarse-grained chain [18]. The occupancy of the three rotational isomeric states is nearly independent of T over the range covered, with 56% of the C–C bonds in *trans* (t) states, and the remainder of the bonds split nearly evenly between the two *gauche* (g^+ and g^-) states.

The 3_1 helix of iPP has a conformation in which g placements of the same sign alternate with t placements. The T dependence of the presence of one, two, or three consecutive repetitions of this sequence is depicted in Fig. 4. The *tg* content of iPP increases with a decrease in T, and there is an increase in the tendency to string the *tg* sequences together, as shown by the doubling of the content of *tgtgtg* upon cooling from 473 to 293 K. However, the content of *tgtgtg* remains near the result expected from the rotational isomeric state model, and does not rise to the much larger value expected for a highly crystalline sample of iPP, due to the fact that 8 million MCS permits time for an equilibration of the local conformations, but does not permit sufficient time for the reorganization and reorientation of the chains that is required for the stabilization of a crystal by intermolecular interactions. Nevertheless, the simulation does provide occasional examples of a chain in which there is side-by-side interaction of helical segments, as shown in Fig. 5.

The probability for *tgtgtg* has a much weaker temperature dependence in the simulation of elPP than in the simulation of iPP. However, it is possible to find a few instance, where a chain of elPP does exhibit segments with recognizable helical content, as shown by the example pictured in Fig. 6. In contrast to the iPP chains, an elPP chain may exhibit a few segments that approach full

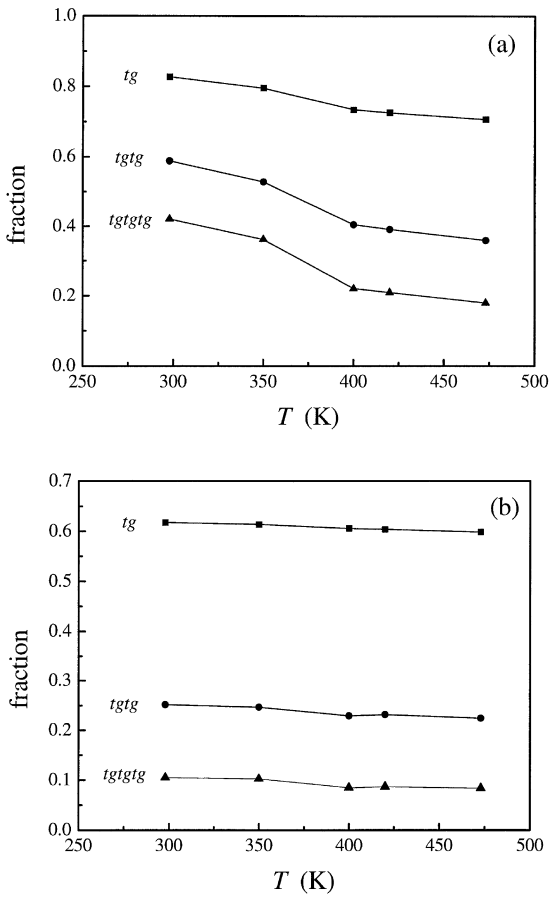

Fig. 4. Dependence on T of the populations of 2, 4, and 6 consecutive C–C bonds in helical *tg* (*gauche* states of the same sign) conformations in (a) iPP and (b) elPP.

extension, as is also shown in Fig. 6. Sequences of several consecutive *t* states are strongly disfavored in iPP, but they readily appear in the strings of *racemo* diads that sometimes occur in the atactic blocks of elPP. (The result is not shown here.)

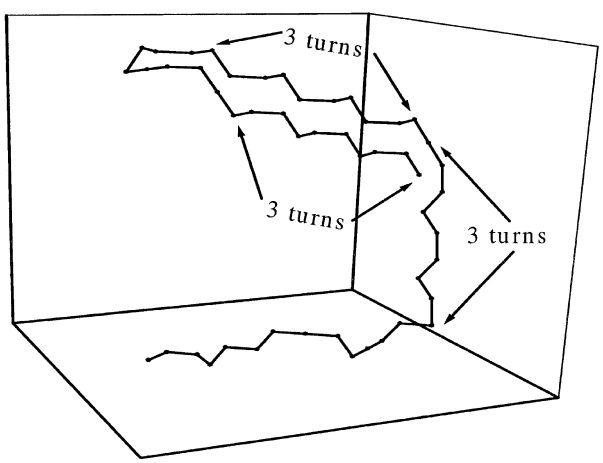

Fig. 5. An example of an iPP chain containing short helical segments, from the simulation at 298 K.

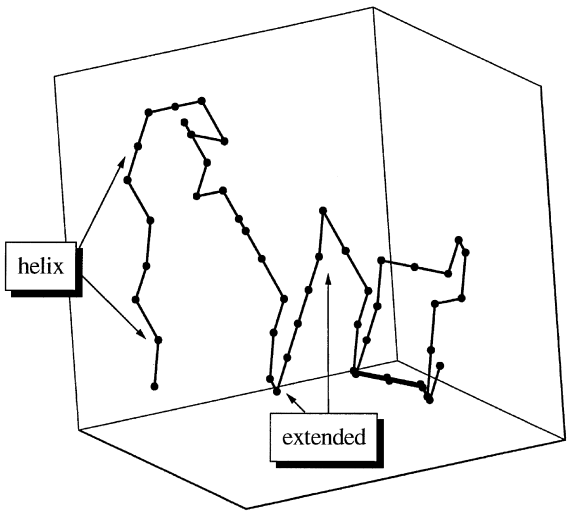

Fig. 6. An example of an elPP chain (chain 7 from Table 3) with a short helical segment and a fully extended segment, from the simulation at 298 K.

3.3. Average local packing of the chains

The local intermolecular packing is obtained from the pair correlation function evaluated from the probability of finding a particle A in a specific shell about another particle A. On the discrete space of the high coordination lattice, with $10i^2 + 2$ sites in shell i, the pair correlation function is defined with Eq. (6)

$$g_{AA}(i) = \frac{\langle n_{AA}(i) \rangle}{(10i^2 + 2)V_A} \tag{6}$$

The number occupancy of A in the ith shell from another A is denoted by $n_{AA}(i)$, the angle bracket means the ensemble average, and V_A is the volume fraction of A in the entire system. We ignore the beads on the same chain that are separated by only one or two coarse-grained bonds from the reference bead. Two sets of results are depicted in Fig. 7. One set uses all of the beads of elPP, and the other set uses only those beads in the *meso* blocks, defined as a string of at least four *meso* diads. Both types of correlation functions exhibit similar behavior. The maximum occurs in the third shell, as expected from the location of the minimum in the Lennard-Jones potential. This maximum increases in size as T decreases. At 298 K, there is a slight increase in the pair correlation function for shells 4–6. Comparison of the two panels in Fig. 7 provides little evidence for a preference of the *meso* blocks to interact with one another when the simulation allows insufficient time for the development of stable crystals.

3.4. Distribution of instantaneous local properties about the average

The characterization of the systems in Figs. 1–4 and 7 uses properties that are averages over the entire system. Here we change the focus of attention to the sizes of the

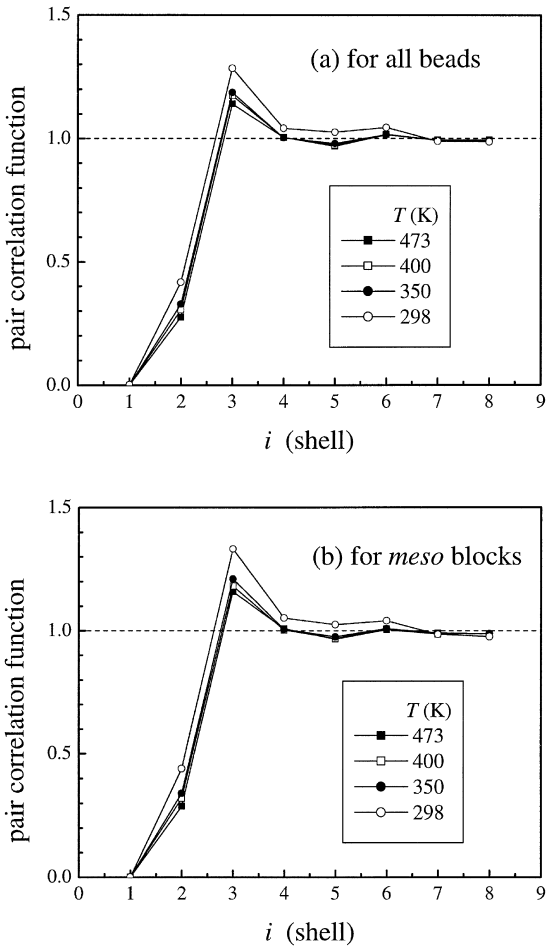

Fig. 7. Intermolecular pair correlation functions for elPP at 298, 350, 400, and 473 K, using (a) all beads, and (b) only those beads in the *meso* blocks.

spatial fluctuations about these averages. It is these fluctuations that become pertinent when one looks for the development of heterogeneity in a system. We look first for heterogeneity in the orientations of closely spaced pairs of coarse-grained bonds, and then for heterogeneity in the local, short-time dynamics.

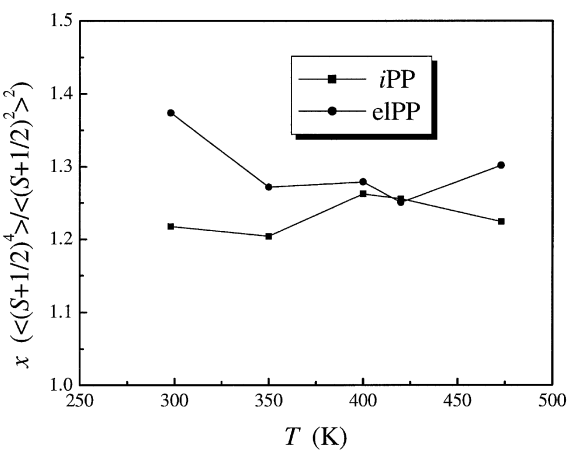

Fig. 8. The parameter x, defined in Eq. (7), for elPP and iPP.

For an assessment of the heterogeneity of the local conformations, we begin with the usual order parameter, $S = (1/2)(3\cos^2\theta - 1)$, defined by the angle, θ, between a coarse-grained bond in one chain and a neighboring coarse-grained bond in another chain. This order parameter is averaged over all bonds within the first three shells about the reference bond. The physically accessible range for this average is from $-1/2$ to 1. For present purpose, we add 1/2 to all values, which shifts the physically accessible range into the positive numbers, from 0 to 3/2. Then we calculate the term x by averaging the values of the shifted order parameter over all choices for the reference bond

$$x = \frac{\langle (S + 1/2)^4 \rangle}{\langle (S + 1/2)^2 \rangle^2} \tag{7}$$

As defined, x measures the size of the variation in the values of S as the choice of reference bond is changed. The values of x for iPP and elPP are compared in Fig. 8. This dimensionless value stays within the range 1.24 ± 0.04 for iPP, and it remains very close to this range for elPP at 350–473 K. The breadth of the distribution of the values of S is similar in these simulations. A larger value for x of 1.38 is obtained with elPP at 298 K. This result signifies an increase in the breadth of the distribution for S when elPP is cooled to 298 K, which implies the development of a more heterogeneous structure at this T.

The heterogeneous structure of elPP at 298 K can also be detected with an analysis of the short-time displacement of individual beads. The two panels in Fig. 9 depict the mean square displacements of individual beads, g_{bead}. At 473 K, all eight chains have similar profiles, with the largest values of g_{bead} observed for beads near the chain ends. At 298 K, however, the short-time displacement of a bead varies more strongly, and the nature of the variation is not subject to summary by a simple statement, as was the case at 473 K. Close inspection of the conformations of the individual chains shows that the beads with low mobility at 298 K often lie in 3_1 helices in isotactic block or in short extended sequences in those portions of the atactic blocks that are rich in *racemo* diads.

A more detailed example of the short-time mobility of the beads is depicted in Fig. 10 for chain 7 from Table 3. One conformation of this chain is depicted in Fig. 6. For the short-time frame considered in Fig. 10, the lowest mobilities are in beads 17–24 (stereochemical sequence *mrrmmrrr*) and in beads 36–50, which is dominated by two isotactic blocks. Fig. 6 shows the presence of an extended conformation near bead 20, and a two-turn 3_1 helical structure at the end of the chain. An isotactic block does not necessarily have a very low mobility, as shown by beads 7–12 in Fig. 10.

The function defined with Eqs. (8) and (9) is designed so that it will measure the breadth of the distribution of the short-time mobilities of the beads in shell i about a reference

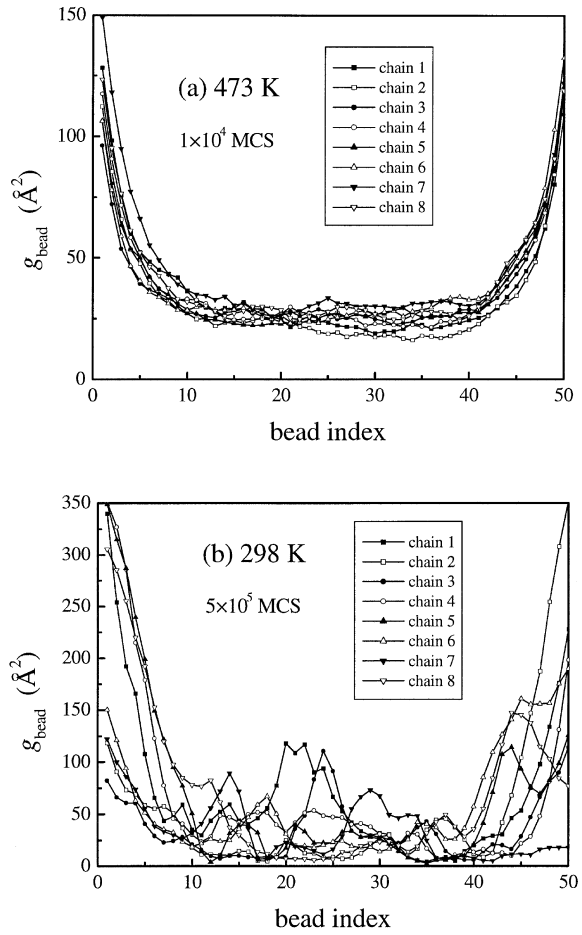

Fig. 9. Mean square displacement of individual beads of elPP at (a) 473 K and (b) 298 K. The stereochemical sequences of the chains are presented in Table 3. The number of MCS at the two temperatures has been adjusted so that both panels produce nearly the same result when g_{bead} is averaged over all beads, and all chains.

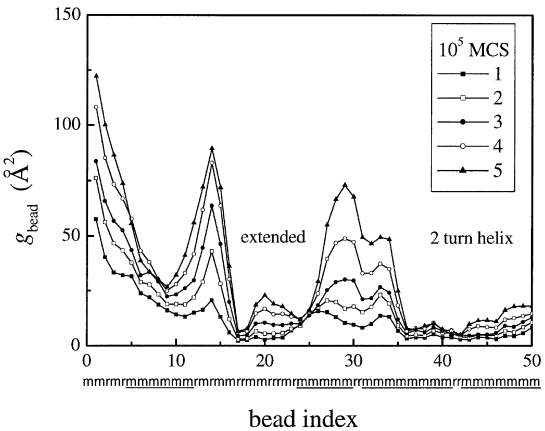

Fig. 10. Mean square displacement of individual beads in a specific chain of elPP (chain 7 from Table 3) at 298 K. The stereochemical sequences is shown under the figure.

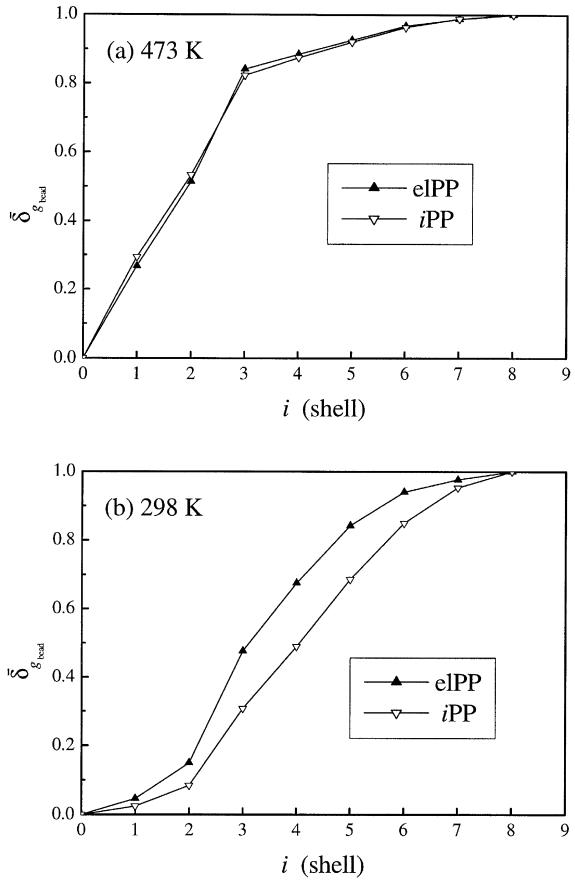

Fig. 11. Spatial distribution of the fluctuation of the mean square displacement of individual beads, defined in Eqs. (8) and (9), for iPP and elPP chains at (a) 473 K and (b) 298 K, using data with a time interval of 1000 MCS.

bead. The numerator of Eq. (8) calculates the fluctuation in g_{bead} for the N_i beads in shell i about a reference bead. It is zero only if all beads in shell i have exactly the same mobility

$$\delta_{g_{\text{bead}}}(i) = \frac{(\langle g^2_{\text{bead}}(i)\rangle - \langle g_{\text{bead}}(i)\rangle^2)^{1/2}}{\langle g_{\text{bead}}(i)\rangle} \tag{8}$$

This fluctuation is then normalized through division by the average of g_{bead} for these N_i beads. The average of $\delta_{g_{\text{bead}}}(i)$ over all choices of the reference beads is denoted by $\langle\delta_{g_{\text{bead}}}(i)\rangle$. At small i, the result depends both on the value of i and on the choice of the reference bead, but the result becomes independent of these choices in the limit as $i \to \infty$. Taking $i = 8$ as an adequate approximation to the limit as $i \to \infty$, we finally focus attention on the term defined in Eq. (9)

$$\bar{\delta}_{g_{\text{bead}}}(i) = \frac{\langle\delta_{g_{\text{bead}}}(i)\rangle}{\langle\delta_{g_{\text{bead}}}(8)\rangle} \tag{9}$$

This term is plotted as a function of shell number, i, in Fig. 11. The two systems exhibit similar behavior at 473 K, but differences in the two systems are apparent at 298 K. At 298 K, the results show that the size of the fluctuation at

shells 2–6 is larger for elPP than for iPP. This result shows that elPP has the larger heterogeneity in the local dynamics. This conclusion for the dynamics is consistent with the more heterogeneous structure of elPP at 298 K, which was deduced from the orientation of pairs of coarse-grained bonds in Fig. 8.

4. Conclusion

When elPP is cooled from its melt, it can develop a heterogeneous structure prior to the onset of appreciable crystallization of the isotactic blocks. This heterogeneous structure can be detected by an analysis of the orientation of coarse-grained bonds, and by an analysis of the short-time local dynamics. Two local conformations contribute to the heterogeneity. One conformation is short 3_1 helices in the isotactic blocks, which have not yet formed stable crystals by specific aggregation with numerous other 3_1 helices. The other conformation is a short extended chain that appears in those portions of the atactic blocks that are rich in *racemo* diads.

The initial development of detectable heterogeneity suggests that aPP and iPP might become immiscible at 298 K, even if crystallization of the iPP could somehow be suppressed. Although experiments with readily accessible samples show that aPP and iPP are miscible in the melt [10,13], there has been a suggestion that the melt might become immiscible if the molecular weight of the components could be increased to several million [13], which is higher than the molecular weights of the components of the systems that have been studied. Therefore, it would not be surprising to find that the hypothetical 'melt' at 298 K should develop inhomogeneity (without crystallization of the iPP) for chains of low molecular weight. In the elPP at 298 K, the initial development of inhomogeneity might arise for this reason, with crystallization of the iPP blocks taking place after the development of the local inhomogeneity arising from the tendency for demixing of aPP and amorphous iPP at 298 K.

Acknowledgements

This research was supported by National Science Foundation grant DMR 0098321.

References

[1] Soga K, Shiono T. Ziegler–Natta catalysts for olefin polymerizations. Prog Polym Sci 1997;22:1503.
[2] Bravakis AM, Bailey LE, Pigeon M, Collins S. Synthesis of elastomeric poly(propylene) using unsymmetrical zirconocene catalysts, marked reactivity differences of 'rac'- and 'meso'-like diastereomers. Macromolecules 1998;31:1000.
[3] Carlson ED, Krejchi MT, Shah CD, Terakawa T, Waymouth RM, Fuller GG. Rheological and thermal properties of elastomeric polypropylene. Macromolecules 1998;31:5343.
[4] Gauthier WJ, Collins S. Elastomeric poly(propylene), propagation models and relationship to catalyst structure. Macromolecules 1995; 28:3779.
[5] Chien JCW, Iwamoto Y, Rausch MD, Wedler W, Winter HH. Homogeneous binary zirconocenium catalyst system for polypropylene polymerizations. 1. Isotactic/atactic interfacial compatabilized polymer having thermoplastic elastomeric properties. Macromolecules 1997;30:3447.
[6] Yu H, Krejchi MT, Shah CD, Myers CL, Waymouth RM. Elastomeric polypropylenes from unbridged (2-phenylindene) zirconocene catalysts. Macromolecules 1998;31:6908.
[7] Madkour TM, Mark JE. Modeling of crystallization in stereoblock polypropylene. Idealized structure showing the effect of isotactic block lengths and their polydispersity. Polymer 1998;39:6085.
[8] Madkour TM, Mark JE. Simulation on crystallization in stereoblock poly(propylene): idealized structure showing the effect of atactic block length. Macromol Theor Simul 1998;7:69.
[9] Clancy TC, Pütz M, Weinhold JD, Curro JG, Mattice WL. Mixing of isotactic and syndiotactic polypropylenes in the melt. Macromolecules 2000;33:9452.
[10] Lohse DJ. The melt compatibility of blends of polypropylene and ethylene–propylene copolymers. Polym Engng Sci 1986;26:1500.
[11] Thomann R, Kressler J, Setz S, Wang C, Mülhaupt R. Morphology and phase behavior of blends of syndiotactic and isotactic polypropylene. 1. X-ray scattering, light microscopy, atomic force microscopy, and scanning electron microscopy. Polymer 1996;37: 2627.
[12] Thomann R, Kressler J, Rudolf B, Mülhaupt R. Morphology and phase behavior of blends of syndiotactic and isotactic polypropylene. 2. Differential scanning calorimetry, light transmission measurements, and PVT measurements. Polymer 1996;37:2635.
[13] Maier RD, Thomann R, Kressler J, Mülhaupt R, Rudolf B. The influence of stereoregularity on the miscibility of poly(propylenes). J Polym Sci, Part B: Polym Phys 1997;35:1135.
[14] Baschnagel J, Binder K, Doruker P, Gusev AA, Hahn O, Kremer K, Mattice WL, Müller-Plathe F, Murat M, Paul W, Santos S, Suter UW, Tries V. Bridging the gap between atomistic and coarse-grained models of polymers, status and perspectives. Adv Polym Sci 2000; 152:41.
[15] Clancy TC, Mattice WL. Role of the attractive portion of the Lennard-Jones potential in the homogeneity of melts of isotactic and syndiotactic polypropylene. J Chem Phys 2001;115:8221.
[16] Xu G, Clancy TC, Mattice WL, Kumar SK. Increase in the chemical potential of syndiotactic polypropylene upon mixing with atactic or isotactic polypropylene in the melt. Macromolecules 2002;35:3309.
[17] Rapold RF, Mattice WL. New high-coordination lattice model for RIS polymer chains. J Chem Soc, Faraday Trans 1995;91:2435.
[18] Haliloglu T, Mattice WL. Mapping of rotational isomeric state chains with asymmetric torsional potential energy functions on a high coordination lattice, application to polypropylene. J Chem Phys 1998; 108:6989.
[19] Orwoll RA. In: Mark JE, editor. Physical properties of polymers handbook. Woodbury, NY: American Institute of Physics; 1996. p. 81.
[20] Metropolis N, Rosenbluth AW, Rosenbluth MN, Teller AH, Teller E. Equation-of-state calculations by fast computing machines. J Chem Phys 1953;21:1087.
[21] Suter UW, Pucci S, Pino P. Epimerization of 2,4,6,8-tetramethylnonane and 2,4,6,8,10-pentamethylundecane, low molecular weight compounds of polypropylene. J Am Chem Soc 1975;97:1018.
[22] Reid RC, Prausnitz JM, Poling BE. The properties of gases and liquids, 4th ed. New York: McGraw-Hill; 1987. p. 734.
[23] Cho J, Mattice WL. Estimation of long-range interactions in coarse-grained rotational isomeric state polyethylene chains on a high coordination lattice. Macromolecules 1997;30:637.

[24] Doruker P, Mattice WL. Reverse mapping of coarse-grained polyethylene chains from the second nearest neighbor diamond lattice to an atomistic model in continuous space. Macromolecules 1997;30:5520.
[25] Clancy TC, Mattice WL. Rotational isomeric state chains on a high coordination lattice: dynamic Monte Carlo algorithm details. J Chem Phys 2000;112:10049.
[26] Madkour TM, Mark JE. Mesoscopic modeling of the polymerization, morphology, and crystallization of stereoblock and stereoregular polypropylenes. J Polym Sci B 2002;40:840.
[27] Tries V, Paul W, Baschnagel J, Binder K. Modeling polyethylene with the bond fluctuation model. J Chem Phys 1997;106:738.